END-TO-END MODELING OF THE SOLAR TERRESTRIAL SYSTEM

M. WILTBERGER[1,*] and D. BAKER[2]

[1]*National Center for Atmospheric Research 3080 Center Green Place Boulder, CO 80301, USA*
[2]*Laboratory for Atmospheric and Space Physics 1234 Innovation Drive, Boulder, CO 80301, USA*
*(*Author for correspondence: E-mail: wiltbemj@ucar.edu)*

Abstract. Traditionally modeling for space science has concentrated on developing simulations for individual components of the solar terrestrial system. In reality these regions are coupled together. This coupling can be as simple as the driving of the magnetosphere – ionosphere – thermosphere system by the solar wind or as a complicated as the feedback of the ionospheric conductivity and currents on the magnetosphere. As part of the CISM project we are beginning a concentrated effort to compressively model the entire system. This approach includes chains of models. In the first chain physics based numerical models are utilized while in the second chain empirical models are coupled together. The first half of this paper discusses the numerical modeling approach by highlighting the coupling of pairs of regions within the system. In the second section we present results from empirical models which are combined to make long term forecasts of conditions in the geospace environment. It is expected that a validated and reliable forecast model for space weather can be obtained by combining the strongest elements of each chain.

Keywords: space physics, numerical modeling, solar physics, magnetospheric physics, ionospheric physics

1. Introduction

Advances in modeling the Earth's weather and climate have required the development of models which couple our understanding of the interactions between the atmosphere, ocean, and land into a single comprehensive model. The long term success of this approach forms the basis of the modeling approach for solar – terrestrial system laid out in the United States National Space Weather Plan. Instead of treating each region of the system separately they will be linked together into a single model capable of describing the entire system and the interactions between regions.

Development of a comprehensive solar-terrestrial model requires the utilization of models for the solar corona, solar wind, magnetosphere, inner magnetosphere, ionosphere and thermosphere. While other groups have conducted work in coupling all (Groth *et al.*, 2000) or a subset (Raeder *et al.*, 2001) of the components together, this paper highlights the work conducted by the Center for Integrated Space Weather Modeling (CISM). The coupling of physics based models together can be augmented in two ways by working with empirical models. First empirical models can serve as baseline for assessing the accuracy and improvements in the

physical models. In addition, an optimal forecast model can be built from linking the strongest components of each model coupling chain into a single comprehensive end-to-end model.

   This paper is divided into two main sections. The first section covers the results from the numerical modeling chain. These results are presented in a series of subsections which deal with the details of couplings between regions in a pairwise fashion. In the second section we discuss the empirical modeling chain. The details of making a solar wind prediction from an empirical coronal model are presented in the first subsection. Empirical modeling for the radiation belts is used to describe the techniques required for simulating the response of geospace to solar wind driving. The paper concludes with a few remarks about tools and techniques that increase the utility of end-to-end modeling.

2. Numerical Modeling

To build a numerical model for space weather prediction which extends from the Sun to the Earth, it is necessary to break the region down into manageable pieces. In Figure 1 an initial breakdown of the region into components is shown. A solar corona model is used to simulate the region in which solar transient events, e.g. flares and coronal mass ejections, begin their initial propagation out into the he-
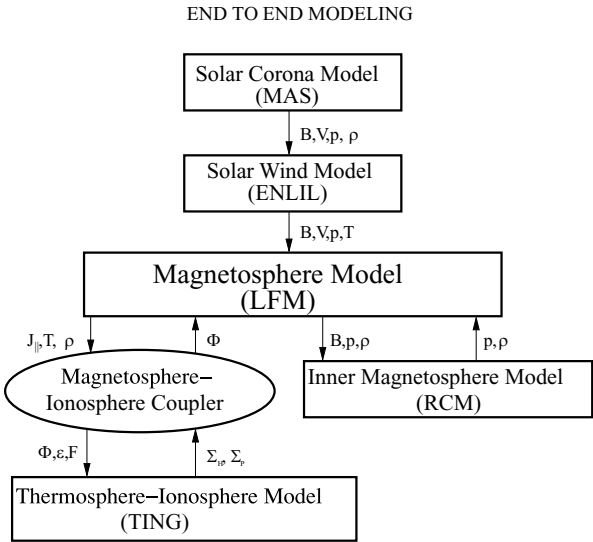

Figure 1. A schematic breakdown of the Sun – Earth system into component modeling regions. The arrows represent information flow with the parameters begin passed between models indicated next to each arrow.

liosphere. It is important to note that this model also plays an important role in specifying the structure of the magnetic topology of the Sun which governs location of the heliospheric current sheet and the location of slow and fast flows in the solar wind. The solar wind model takes information about the state of the plasma near the Sun, typically around 30 solar radii, from the solar corona model and propagates it out into the heliosphere. The coupling between these two models is fairly straight forward and usually involves passing specification of the plasma at a two-dimensional interface from the solar corona model to the solar wind model.

The modeling within the magnetosphere – ionosphere – thermosphere system is considerably more complicated because of the interconnection between these regions. The coupling between the solar wind model and the magnetospheric model requires specification of the plasma parameters along the entire computational domain of the magnetosphere. At resolutions that are practical with modern computers this typically means producing a one-dimensional solar wind stream similar to spacecraft observations, but as computing power and computational techniques advance this will become a three-dimensional problem. The magnetospheric model needs to specify the plasma and magnetic field parameters throughout a region that extends from close to the ionosphere to beyond the magnetopause and bow shock in all three-dimensions. Since taking the physical parameters involves a utilization of a set of models we break this process out into a separate interface coupler as indicated by the ellipse in Figure 1.

The most complicated coupling in this system is the interchange of information between the magnetosphere model and inner magnetosphere model which provides an accurate representation of the ring current and plasmasphere. It involves the specification of three-dimensional magnetic field structure in a subset of the closed field region within the magnetosphere. In this region the magnetosphere model provides an initial guess as to the structure of the plasma pressure and density which is then modified by the inner magnetosphere model and fed back in along the magnetic field lines. Coupling between geospace models is obviously quite tight and must be handled with considerable care in order to ensure the stability of the individual models and the reliability of the results.

Figure 1 is schematic, illustrating only an initial set of models necessary to represent the Solar – Terrestrial system. It can be expanded to include several additional models. Emergence of magnetic flux from beneath the photosphere and its evolution into structures which can erupt as CMEs may require the addition of regional models within the domain covered by the solar corona model. Specification of the radiation belts within the magnetosphere requires tracking highly energetic particles within the magnetosphere. Entry of solar energetic particles into the magnetosphere and thermosphere requires an understanding of the processes controlling their generation, propagation through the heliosphere, and transport through the topology of the magnetic field in geospace. All of these aspects can be thought of as additional rectangles in the modeling schematic which requires the

creation of couplers to keep the interfaces clean and to facilitate easily inclusion of other approaches.

As part of the efforts by the CISM, individual models for each of the physical regions have been selected to form the comprehensive physical model. The Magnetohydrodynamics Around a Sphere (MAS) (Linker and Mikic, 1995; Mikic *et al.*, 1999) model is used to model the solar corona. The ENLIL model developed by Odstrcil and Pizzo, 1999, simulates the solar wind propagation through the heliosphere. The Earth's magnetosphere is modeled using the Lyon – Fedder – Mobbary (LFM) code (Fedder *et al.*, 1995; Lyon *et al.*, 2004) with the inner magnetosphere being simulated by the Rice Convection Model (RCM) (Harel *et al.*, 1981; Wolf, 1983; Toffoletto *et al.*, 2003). The Thermosphere Ionosphere Nested Grid (TING) model (Wang *et al.*, 1999) is used to simulate the upper atmosphere and ionosphere. In the remainder of this section we will provide a brief overview of the pairwise couplings that make the chain of models in the solar terrestrial physics system.

2.1. SOLAR CORONA AND SOLAR WIND COUPLING

The MAS model is used to simulate the solar corona. It uses magnetohydrodynamic (MHD) equations to model the plasma on a spherical computational grid which extends from the photosphere out to 30 solar radii. The model uses global photospheric magnetic field maps, which can be purely theoretical or obtained from magnetograms, to determine the boundary conditions. More detail about these boundary conditions and their temporal evolution can be found in Mikic *et al.* (1999). As described in Linker *et al.* (1999) the model uses a polytropic equation of state, with $\gamma = 1.05$, which helps produces a density and flow differential on open and closed field lines. Unfortunately this physical simplification does not include effects like Alfven wave heating and results in the model having outflow speeds and gradients between high and low speeds which are considerably smaller than observed. It is important to note that the outer boundary is beyond the critical point so that the flow is supersonic.

The ENLIL solar wind model is designed to study the motion of supercritical plasma and magnetic field evolution throughout the heliosphere. It uses the MHD equations with a polytropic equation of state. In this case it uses a a value of $\gamma = 1.5$. The computational domain extends from a region beyond the critical point near the Sun to as far out into the heliosphere as desired. In order to reduce the computational work load and optimize resolution the latitude extent is limited to a region $\pm 60°$ from the equator.

Since the coupling between these models has been discussed in great detail in Riley *et al.* (2001b), Odstrcil *et al.* (2002) and Odstrcil *et al.* (2004) we will only provide brief overview of the process here. The solar corona model is run for a period of time and the data are transfered to the ENLIL model, where a small spherical shell of a few grid cells is used to determine the MHD state vector at the grid points along
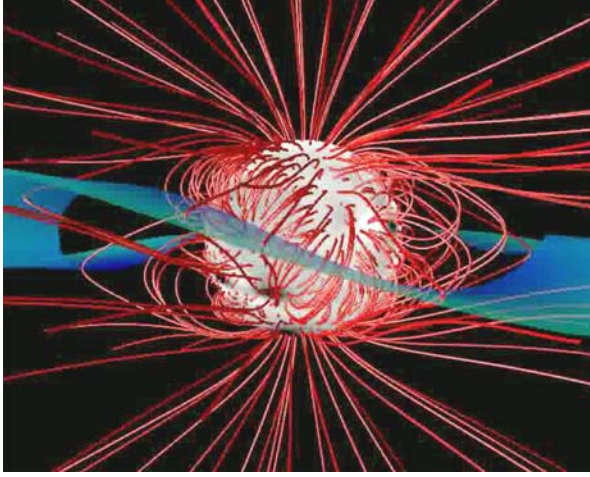
Figure 2. Image from a MAS simulation for Carrington rotation 1923. The event was driven by synoptic magnetic field maps seen on the photospheric surface in the image. Red magnetic field lines show an open region near the poles and streamer belt. The heliospheric current sheet is distorted by the magnetic topology and is colored by the local solar wind velocity. Courtesy Sarah McGregor.

the inner boundary of the computational domain. At this point several additional changes are made to the plasma parameters to improve the physical accuracy of the coupling. First, the coronal model is rotated by a discrete amount between each time step in order to create a Parker spiral distorted heliospheric current sheet as seen in Figure 2. Since the MAS simulations have a solar wind speed that is lower than observed it is also adjusted by a correction factor dependentupon the magnetic field topology. Using this inner boundary condition information allows ENLIL to specify the plasma parameters through the heliosphere, including at the Earth where it is used to drive the geospace models.

2.2. MAGNETOSPHERE AND IONOSPHERE - THERMOSPHERE COUPLING

To model the magnetospheric plasma configuration another MHD model, the LFM (Lyon *et al*., 2004), is used. The LFM computational domain covers a roughly cylindrical region embedded in the solar wind that extends from 30 R_E upstream to 300 R_E downstream of the Earth. The radial extent is typically 100 R_E. At the position of the Earth a small sphere is cut out which is typically between 2–3 R_E in radius. The boundary conditions along the outer edges are specified by the solar wind conditions. At the inner boundary MHD parameters are mapped down to ionospheric heights where they are used to determine the cross polar cap potential which is used as the flow boundary condition for the magnetospheric plasma. When operating in a stand-alone mode this calculation is done within a simple two-dimensional electrostatic model for the ionosphere.

The coupled thermosphere-ionosphere system is modeled by the Thermosphere Ionosphere Nest Grid model which solves for the coupled equations for mass, momentum, and energy for neutrals and O^+ in this domain (Wang *et al*., 1999, 2004). Chemical equilibrium is used to determine the density of other ion species, e.g. NO^+, O_2^+, and the electrons. The model has the capability to include nested grid structures within its regular latitude-longitude grid for improved regional resolution. The vertical domain extends from 97 to 500 km with 25 constant pressure levels. It uses the F10.7 flux to determine the EUV ionization. It needs the energy flux of precipitating electrons and a polar cap convection pattern to be specified. Finally, it needs to have the tides from the lower atmosphere specified at 97 km altitude. In stand-alone operation the magnetospheric parameters are determine from empirical models.

The coupling of these two models forms the Coupled Magnetosphere Ionosphere Thermosphere (CMIT) model which is described in detail in Wiltberger *et al*. (2004) and Wang *et al*. (2004), so once again we will only provide a brief overview. Since the transfer of information between these two models is bidirectional and involves the transformation of different sets of physical parameters, we decided to separate these functions into a discrete coupling module. Currently this module is closely linked with the LFM, but it can removed and placed into other models in a straight forward fashion. This module takes the plasma parameters along the inner boundary of the MHD domain and transforms them into the precipitating electron energy flux using empirical relationships discussed in Slinker *et al*. (1995). Using the previous information from the TING model it makes an initial guess for the ionospheric convection pattern which is passed along to the model with electron information to determine a conductance distribution. The new conductance information is used to compute a new potential pattern which is used as the boundary condition for the MHD domain. There is a large disparity in time steps between these two computational domains, which we utilize to our advantage. In TING a typical time step is two minutes, while in the LFM a typical time step is 0.3 sec. In CMIT, the LFM portion uses the conductance information for a two minute interval while recomputing the potential pattern based upon the current field aligned current configuration. At the end of that interval, another information exchange between the models occurs and the conductivities are updated for the next two minute interval. Originally, we thought that it might be necessary to iterate the exchange between these two models to prevent large changes in the convection pattern from being seen by TING, but that has not turned out to be necessary in practice.

Results from the coupled model are shown in Figure 3. The simulation was driven by solar wind parameters taken from an end-to-end event study described in Luhmann *et al*. (2004). The high density and southward IMF results in a strong compression of the dayside magnetopause which can be seen by the red high density region in the Figure. Reconnection is occurring along the dayside which results in open field lines being created in the polar cap. At the ionospheric altitude a strong
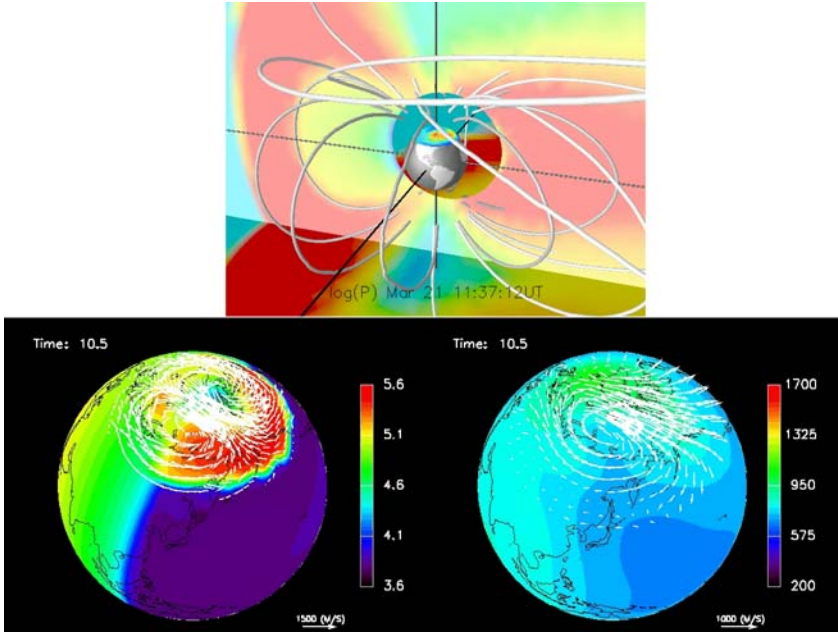
Figure 3. The top panel shows an image from the CMIT simulation which shows the plasma density on equatorial and meridional cut planes through the computational domain. A series of magnetic field lines are drawn in white including several open ones. At the ionospheric altitude the Hall conductance as determined by TING is displayed during the strong driving of magnetic storm. On the bottom left we see the we see the electron density in the E region with the ion drift (convection) pattern superposed on top. On the right hand side we see the F region temperature and the neutral winds.

enhancement to the Hall conductance in the auroral zone is clearly evident. This storm produces strong effects in the thermosphere, e.g. heating of the F region and enhanced neutral winds, which are discussed in Wang *et al*. (2004) and are summarized in the bottom panel of Figure 3. On the left hand side we see ion drifts in the E region of the ionosphere as imposed by the magnetospheric portion of the CMIT model. The color scale shows the electron density with significant enhancements present in the auroral zone. Strong driving results in higher neutral temperatures in the F region as seen the lower right portion of the figure. In addition, the strong ion drifts are driving neutral winds at F region altitudes which show the characteristic rotation enhancement on the dawnside.

2.3. MAGNETOSPHERE AND INNER MAGNETOSPHERE COUPLING

The Rice Convection Model uses the Vasyliunas, 1970, approach of using drift and current conservation equations to determine the plasma motion, currents, and electric fields in the inner magnetosphere. It assumes an isotropic distribution of

particles on closed field lines and considers time scales for the drifts to be longer than other time scales in the system. The model also requires that the magnetic field configuration in the inner magnetosphere be specified. A detailed description of this numerical technique can be found in Toffoletto *et al.* (2003). The essential point here is that the model uses the flux tube volume to track the drift motion of the slices of the plasma distribution function for several species. This information can be converted back into a plasma pressure and density which is constant throughout the flux tube.

The MHD approach of the LFM and the multi-species kinetic approach of the RCM are in fact quite complementary. The RCM provides an excellent description of the inner magnetosphere including the effects of ionospheric shielding, formation of region 2 currents. However, it does not provide a self consistent description of the magnetic field. The LFM provides a magnetic field configuration which is necessarily consistent with the plasma configuration, but it does not well represent the gradient and curvature drift physics. This results in weak region 2 currents and little enhancement of the ring current during magnetic storms. In the two-way coupled model, the LFM provides RCM with a magnetic field configuration in the inner magnetosphere along with initial values for the plasma pressure and density. The RCM assumes a Maxwellian distribution for the plasma and uses it as time-dependent boundary conditions for a drift calculation. This calculation is not required to preserve the Maxwellian character of the distribution. These plasma parameters are then passed back to the LFM with the assumption that the density and pressure determined by the RCM is constant along each field line. The core of this coupling requires transferring information between the regular spatial grid of the LFM and the flux tube volume representation of the RCM. It is accomplished by tracing field lines on a rectangular grid, with source points that originate from the regular ionospheric grid in the RCM.

A comparison between the stand-alone LFM and the coupled LFM-RCM model is shown in Figure 4. Each model was run for a configuration which has the interplanetary magnetic field turning southward at 4UT and remaining southward for the remainder of the simulation. In the left-hand panel we see the LFM configuration at 6 UT with coupled model results at the same time shown in the right hand panel. In each panel the color contours show the plasma pressure with the same color bar. Magnetic field lines, shown in white, are drawn from the same locations along the X axis. In both models what appears to be a substorm has already occurred. In the stand alone LFM the field in the inner magnetosphere is primarily dipolar, with minimal enhancement of the pressure in the inner magnetosphere. In the coupled model the field shows a more stretched configuration, with significant enhancement of the inner magnetospheric pressure. This pressure spreads out in both local time and radial extent as the interval progresses, indicating the development of a significant ring current in the coupled simulation results.
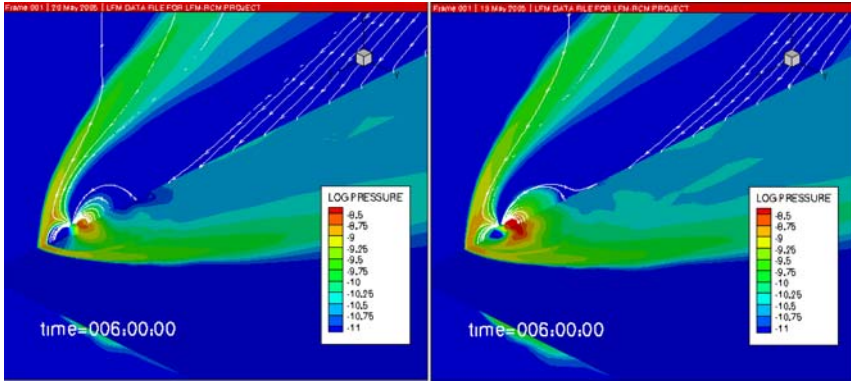
Figure 4. This figure compares results for the pressure (colored contours) and the magnetic field (white lines) configuration between the stand alone LFM (left) and the two-way coupling between the LFM and RCM (right). A clear enhancement of the inner magnetospheric pressure in the inner magnetosphere is present indicative of a improve representation of the ring current. The magnetic field lines show inflation caused by the larger ring current.

3. Empirical Modeling

While building a physics-based numerical model for the Solar-Terrestrial system is a key goal of the CISM project, this effort is augmented by efforts to build a forecast model from empirical, semi-empirical and inverse models. In addition to providing forecasts which may be of utility to the Space Weather community the coupling of these models together will provide a baseline which can be used to assess the accuracy and robustness of the physics-based model.

As with the physics-based models, the key to making predictions about the state of the geospace environment is to understand the conditions in the solar wind. The top path in Figure 5 shows the typical prediction route where measurements of the solar wind density (ρ), velocity (**V**), and magnetic field (**B**) are propagated to the Earth. These measurements can be used to drive models to predict the MeV electron flux (Vassiliadis *et al.*, 2002; Li *et al.*, 2003), magnetic field configuration (Tsyganenko, 1995), ground magnetic field perturbations (Weigel *et al.*, 2003), and the vast array of magnetic indicies (Kp, Ap, Dst, AE) (Boberg *et al.*, 2000; McPherron, 1999; Klimas *et al.*, 1998; Takalo and Timonen, 1997). In the bottom path data input is pushed back to the solar surface where observations of the photospheric magnetic field are used within the Wang – Sheeley – Arge (WSA) method (Arge and Pizzo, 2000) to determine the solar wind speed and limited information about the interplanetary magnetic field at 1 AU. Using this path allows for earlier lead times in the predictions; however as we will see, it greatly decreases the accuracy of the predictions at the Earth. In the remainder of this section we will briefly explore some of these empirical models and their ability to predict the configuration of the Sun-Earth system.
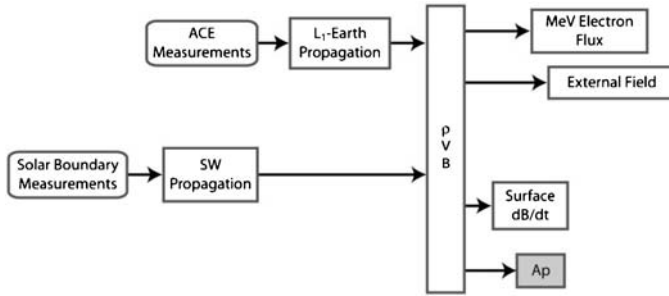
Figure 5. A schematic representation of the coupling of observations to empirical models for pre-
dicting the state of the magnetosphere.

3.1. SOLAR WIND MODELING

The empirical modeling of the solar wind provides information about the ambient
solar wind speed and interplanetary magnetic field polarity throughout the helio-
sphere. It is important to note that this kinematic model provides information about
the quasi-steady solar wind flow and will therefore have greater accuracy for recur-
rent phenomena than for transients. The original Wang and Sheeley (WS) model
(Wang and Sheeley, 1992) used ground-based line-of-sight observations of the solar
surface magnetic field as input to a potential magnetic field model (PFSS (Schatten
et al., 1969) of the coronal magnetic field configuration. The expansion of magnetic
field from the photosphere to a spherical surface at 2.5 solar radii is used to drive
an empirical model for determining the solar wind speed at this surface (Wang and
Sheeley, 1990). The model then assumes that solar wind flow propagates radially
outward from this surface with all subsequent interactions ignored.

Several improvements have been made to the original WS model over the years
and are incorporated into the WSA version of the model. These improvements are
discussed in detail by Arge *et al.* (2004) so we will only provide a brief overview of
them here. The first category of modifications include improvements to the way the
input photospheric magnetic field is processed. These include accounting for line of
sight projection effects, polar field values, line-saturation effects in the creation of
global synoptic maps from the raw magnetograms. They also developed techniques
for making frequent updates to the synoptic map and the handling of data gaps.
The WSA version contains several improvements to the physical model itself.
This includes utilization of a slightly more sophisticated propagation model which
allows for interactions between the streams. A higher-accuracy empirical model for
determining the solar wind speed was created by utilizing a fit to L1 observations.
In addition, the model was further improved by including information about the
distance between the open field line and the nearest coronal hole boundary (Riley
et al., 2001a). These modifications result in significant increases in the prediction
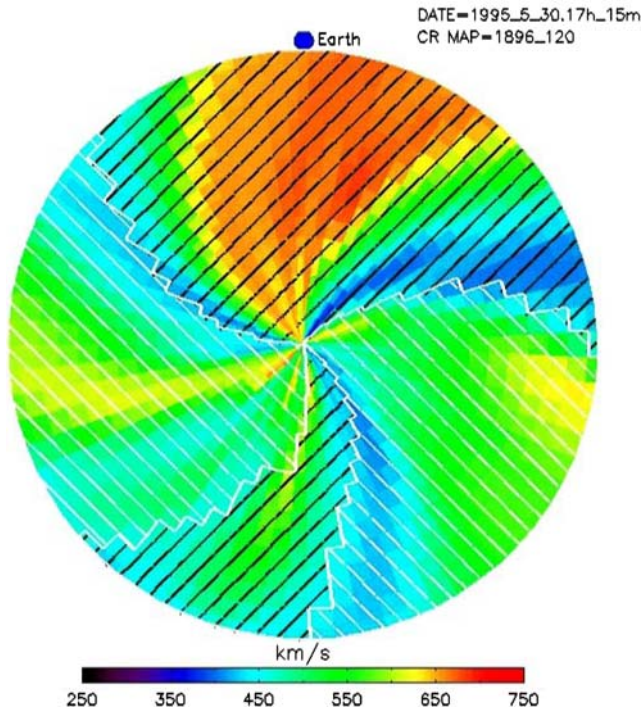efficiency of the the model.

Figure 6. Results from the WSA model for Carrington Rotation 1896. Color indicates speed, while magnetic field polarity toward(away) is indicated by the white(black) lines. Regions of magnetic field toward/away the sun are covered with black/while lines. The location of the Earth is shown with a blue sphere.

Figure 6 shows the results for the WSA model during Carrington rotation 1896. It is clear that a series of high speed streams are reaching the Earth. In other portions of the heliosphere the solar wind speed is quite low. The figure also indicates regions of magnetic field pointed toward (black lines) the Sun and regions of field pointed away (white lines) from the Sun. A time history of the solar wind speed and polarity is obtained by extracting data from the location of the Earth as the model evolves forward in time. It is important to note this time history has a low cadence of one data point every few hours.

3.2. RADIATION BELT MODELING

Empirical modeling of the response of geospace to solar wind conditions is applied to many parameters that describe the system. In general, these methods can be broken down into two broad categories. A black box system utilizes techniques like neural networks to transform the input parameters into output conditions without requiring any physical understanding of the system. These models can produce reliable results quickly for complex systems. The accuracy of the data is the major

limiting factor, and as such they have difficulty with predictions for events at the limit or outside the range of data used to develop the model. Grey box systems combine qualitative knowledge of the system with data to develop a model for making predictions. These techniques include linear filters and state-space models capable of representing ordinary differential equations (ODE) with coefficients determined from a training data set. The essential characteristics of these techniques are the same whether they attempt to predict Ap or radiation belt flux at geosynchronous orbit. In this section we will limit our discussion to radiation belt flux.

Baker *et al*. (1990) used the linear filter method to predict the average daily flux of electrons, J_e, at geostationary orbit. In a classic application of the grey box philosophy of design they assumed that the dynamics of J_e can be described in part by an ODE with the solar wind velocity, V_{SW}, as a driver. The coefficients of this ODE are derived from a historical data set of V_{SW} and J_e. The result of applying this technique is the generation of an impulse response function (IRF) which describes how the flux responds to a unit increase in solar wind velocity. In this case, the IRF shows that the flux initially experiences a sharp dropout followed by a rise in flux over the two day interval following the impulse. Once the peak is reached the flux levels decay over the next four days until they return to the pre-impulse levels. Vassiliadis *et al*. (2002) applied this technique to a range of L-shells and found a relatively localized peak near L $= R_E$ at one day, and a subsequent peak at 2–3 days that extended from 4–7 R_E consistent with Baker *et al*. (1990) earlier findings.

Baker *et al*. (2004) linked this empirical model for predicting radiation belt fluxes to the WSA model which predicts the value of solar wind speed. They utilized the solar observations for the entire year of 1995 which is near solar minimum and has several recurring high speed streams. These conditions are favorable for the application of the WSA technique. The interval also contained several data gaps and a flat heliospheric current sheet which make predictions more challenging. Comparison of the predictions with L1 measurements have a correlation coefficient of 0.36 and a prediction efficiency (PE) of 0.13. The model clearly captures the trends in the solar wind flow, but has significant errors (± 2 days) in predicting the arrival time of impulses at the Earth. Feeding these solar wind velocity measurements to the empirical model for radiation belt fluxes leads to results with a PE of 0.05 for 3 and 4 days out. This compares to a PE of 0.17 at 3 days and a PE of 0.13 at 4 days for a model based upon old L1 observations. Combining the WSA predictions with observations of solar speed and recent flux levels improves the results to slightly better than the model run on L1 data. This implies that significant limiting factor in the 3 to 4 predictions is the poor PE of the WSA model. It anticipated that as the WSA improves the PE will exceed that of the L1 model.

4. Summary and Conclusions

In this paper we have presented results from numerical and empirical models which have been joined together to make predictions about the state of the coupled

Sun – Earth system. The numerical chain utilizes state-of-the-art regional models and couples them together by passing physical parameters along regions of interface. In some cases these couplings are simple one-way transfers of information along boundaries and in other cases they involve two-way transfers of information in three-dimensional regions of overlap. On the empirical side the coupling of models involves the passing of information from one interface to another. It highlights the fact that resulting model will have an accuracy which is limited by the least accurate model in the coupling chain. As part of the CISM program we envision a close coupling between these two chains. At a minimum, the empirical models can provide a baseline model for assessing the skill of the numerical models as they become operational. In addition, a forecast model will be created which utilizes the strongest components of each chain to make the best possible prediction.

The development of a linked chain of models for the Sun-Earth system highlights the need for a consistent framework for coupling the models together and a set of tools for visualizing and analyzing the results. In Goodrich *et al.* (2004) the details of the CISM framework are discussed. A common method for transferring information between running codes, including the difficult problem of passing information between codes with data distributed amongst several processors, form one pillar of the framework. The second pillar utilizes a package to provide interpolation between various grids by simply defining the location of the grid points at any given point in time. CISM-DX is a package which has been developed for visualizing and analyzing space science model output and observations within a single tool (Wiltberger *et al.*, 2005). It combines the three-dimensional visualization strengths of OpenDX (IBM, 1998) with the Octave (Eaton, 2002) analysis tool. In addition, it includes numerous extensions of each package for space physics applications. The package is released under an open-source licensing agreement and contains examples of analysis which extend from very simple to very complex.

Modeling of the Solar – Terrestrial system does not happen in a vacuum. Our efforts are highly dependent upon the quality and quantity of observations, especially at regions which for the boundaries of the system. Improvements in the specification of the photospheric magnetic field include results from STEREO which will expand our field of view and the Solar Dynamics Observatory which will improve our understanding of the connection between small scale and large scale magnetic structures at the photosphere. Improvements in our physical understanding of the system are also required. Understanding the mechanisms that lead to eruption of CMEs will be essential for making accurate predictions at the Earth. In the terrestrial environment will need to further our understanding of the interaction between waves and particles that lead to acceleration and loss of radiation belt particles. There are many challenges in the future for modeling, but the coupling of these models provides an unprecedented opportunity for understanding the system as a single entity.

Acknowledgements

References

Arge, C. N., Luhmann, J. G., Odstrcil, D., Schrijver, C. J., and Li, Y.: 2004, *J. Atm Solar Terr. Phys.* **66**, 1295.

Arge, C. N., and Pizzo, V. J.: 2000, *J. Geophys. Res.* **105**, 10465.

Baker, D. N., McPherron, R. L., Cayton, T. E., and Kebesadel, R. W.: 1990, *J. Geophys. Res.* **95**, 15133.

Baker, D. N., Weigel, R. S., Rigler, E. J., Vassiliadis, R. L. M. D., Arge, C. N., Siscoe, G. L., *et al.*: 2004, *J. Atm. Solar Tres. Res.* **66**, 1491.

Boberg, F., Wintoft, P., and Lundstedt, H.: 2000, *Physics and Chemistry of the Earth C* **25**, 275.

Eaton, J. W.: 2002, *GNU Octave Manual*. Network Theory Ltd., 1st edition.

Fedder, J. A., Lyon, J. G., Slinker, S. P., and Mobarry, C. M.: 1995, *J. Geophys. Res.* **100**, 3613.

Goodrich, C. C., Sussman, A. L., Lyon, J. G., Shay, M. A., and Cassak, P. A.: 2004, *J. Atm. Solar Tres. Phys.* **66**, 1469.

Groth, C. P. T., DeZeeuw, D. L., Gombosi, T. I., and Powell, K. G.: 2000, *J. Geophys. Res.* **105**(A11), 25053.

Harel, M., Wolf, R. A., Reiff, P. H., Spiro, R. W., Burke, W. J., Rich, F. J., *et al.*: 1981, *J. Geophys. Res.* **86**, 2217.

IBM: 1998, *IBM Visualization Data Explorer User's Guide*. Yorktown Heights, NY USA: IBM, 3rd edition.

Klimas, A. J., Vassiliadis, D., and Baker, D. N.: 1998, *J. Geophys. Res.* **103**(12), 20435.

Li, X., Temerin, M., Baker, D. N., Reeves, G. D., Larson, D., and Kanekal, S. G.: 2003, *Eos Transactions of the AGU* **84**, 369.

Linker, J. A., and Mikic, Z.: 1995, *J. Geophys. Res.* **100**, 25165.

Linker, J. A., Mikic, Z., Biesecker, D. A., Forsyth, R. J., Gibson, W. E., Lazarus, A. J., *et al.*: 1999, *J. Geophys. Res.* **104**, 9809.

Luhmann, J., Solomon, S., Wang, W., and Wiltberger, M.: 2004, *J. Atm. Solar Terr. Phys.* p. doi:10.1016/j.jastp.2004.04.005.

Lyon, J. G., Fedder, J. G., and Mobarry, C. M.: 2004, *J. Atm. Space Phys.* pp. 1333–1350.

McPherron, R. L.: 1999, *Phys. Chem. Earth (C)* **24**((1–3)), 45.

Mikic, Z., Linker, J. A., Schnack, D. D., Lionello, R., and Tarditi, A.: 1999, *Phys. Plasmas* **6**, 2217.

Odstrcil, D. J., Linker, J. A., Lionello, R., Mikic, Z., Riley, P., Pizzo, V. J., *et al.*: 2002, *J. Geophys. Res.* **107**, doi:10.1029/2002JA009334.

Odstrcil, D. J., and Pizzo, V. J.: 1999, *J. Geophys. Res.* **104**, 483.

Odstrcil, D. J., Pizzo, V. J., Riley, J. A. L. P., Lionello, R., and Mikic, Z.: 2004, *J. Atm. Solar Terr. Phys.* **66**, doi:10.1016/j.jastp.2004.04.007.

Raeder, J., Wang, Y., and Fuller-Rowell, T. J.: 2001, In: H. S. and (ed.), *Space Weather*, Vol. 125 of *Geophysical Monograph Series*. AGU, pp. 377–384.

Riley, P., Linker, J., Mikic, Z., and Lionello, R.: 2001a, In: P. Song, H. Singer, and G. Siscoe (eds.), *Space Weather*, Vol. 125 of *Geophys. Mono.* Washington, D.C.: AGU, p. 159.

Riley, P., Linker, J. A., and Mikic, Z.: 2001b, *J. Geophys. Res.* **106**, 15889.

Schatten, K. H., Wilcox, J. M., and Ness, N. F.: 1969, *Solar Physics 9* pp. 442–455.

Slinker, S. P., Fedder, J. A., and Lyon, J. G.: 1995, *Geophys. Res. Lett.* **22**, 859.

Takalo, J., and Timonen, J.: 1997, *Geophys. Res. Lett.* **24**, 2403.

Toffoletto, F. R., Sazykin, S., Spiro, R. W., and Wolf, R. A.: 2003, *Space Sci. Rev.* **107**, 175.

Tsyganenko, N. A.: 1995, *J. Geophys. Res.* **100**, 5599.

Vassiliadis, D., Klimas, A. J., Kanekal, S., Baker, D., and Weigel, R. S.: 2002, *J. Geophys. Res.* **107**, 10.1029/2001JA000506.

Vasyliunas, V. M.: 1970, In: B. M. McCormac (ed.), *Particles and Fields in the Magnetosphere*. Hingham, MA: Reidel, pp. 60–71.

Wang, W., Burns, A. G., Solomon, S., and Killeen, T. I.: 2004, *Adv. Space Res.* p. in press.

Wang, W., Killeen, T. L., Burns, A. G., and Roble, R. G.: 1999, *J. Atm. Solar Terr. Phys.* **61**, 385.

Wang, Y. M., and Sheeley, N. R.: 1990, *Ap. J.* **355**, 726.

Wang, Y. M., and Sheeley, N. R.: 1992, *Ap. J.* **392**, 310.

Weigel, R. S., Klimas, A. J., and Vassiliadis, D.: 2003, *J. Geophys. Res.* **108**, doi:10.1029JA009627.

Wiltberger, M., Wang, W., Burns, A., Solomon, S., Lyon, J. G., and Goodrich, C. C.: 2004, *J. Atm. Solar Terr. Phys.* p. submitted.

Wiltberger, M., Weigel, R. S., Gehmeyr, M., and Guild, T.: 2005, *J. Geophys. Res.* **110**, doi:10.1029/2004JA010956.

Wolf, R. A.: 1983, In: R. L. Carovillano and J. M. Forbes (eds.), *Solar Terrestial Physics*, D. Hingham, MA: Hingham, pp. 303–368.